Applied Surface Science 476 (2019) 174–181

Contents lists available at ScienceDirect

Applied Surface Science

journal homepage: www.elsevier.com/locate/apsusc

Full Length Article

Differential charging effects from impurities in pyrolytic graphite

Víctor G. Baldovino-Medrano[a,b,c,d,*], Rogelio Ospina[a,b,c], Eric M. Gaigneaux[d,*]

[a] Centro de Materiales y Nanociencias (CMN), Parque Tecnológico Guatiguará (PTG), Km. 2 vía El Refugio, Universidad Industrial de Santander, Piedecuesta (Santander) 681011, Colombia

[b] Centro de Investigaciones en Catálisis (@CICAT UIS), Parque Tecnológico Guatiguará (PTG), Km. 2 vía El Refugio, Universidad Industrial de Santander, Piedecuesta (Santander) 681011, Colombia

[c] Laboratorio de Ciencia de Superficies (@Csss_UIS), Parque Tecnológico Guatiguará (PTG), Km. 2 vía El Refugio, Universidad Industrial de Santander, Piedecuesta (Santander) 681011, Colombia

[d] Institute of Condensed Matter and Nanosciences (IMCN), MOlecules Solids and reactiviTy (MOST), Université catholique de Louvain (UCL), Place Louis Pasteur 1, Box L4.01.09, 1348 Louvain-la-Neuve, Belgium

ARTICLE INFO

Keywords:
Pyrolytic graphite
Inorganic impurities
XPS
Differential charging
Flood gun
O 1s

ABSTRACT

This work reports differential charging effects in samples of pyrolytic graphite. Despite being considered a nuisance in XPS analyses, differential charging effects can be exploited for the identification and quantification of chemical species in heterogeneous materials. In this case, charging effects were useful to identify impurities at the surface of pyrolytic graphite. For these impurities, the analysis of the O 1s, Si 2p, and Al 2p core levels allowed distinguishing the contributions of SiO_2 and Al_2O_3 from those of silicone/alumino-silicate oxides. Though both groups of compounds are insulators, a splitting of the above peaks was induced by the use of the flood gun device of the spectrometer when the samples were mounted on a conductive metallic sample holder. The shape and relative concentration of the chemical species ascribed to the split peaks served as a basis for the decomposition of the corresponding O 1s, Si 2p, and Al 2p peaks registered over a ceramic sample holder. The latter allowed for inducing a well controlled differential charging of the samples that led to the identification of true chemical shifts, i.e. those ascribed to variations on the chemical environment of the elements. A qualitative model for describing the observed charging effects was postulated. The model was based on an analogy between electrical circuits and the geometrical configuration of the impurity particles intercalated within the graphite particles.

1. Introduction

X-ray photoelectron spectroscopy (XPS) [1] is nowadays routinely used as a surface characterization technique for solid materials [2]. When using this type of technique, insulators or conductors containing an additional insulator layer at their surface (e.g. oxidized metallic layers) will experience surface positive charge buildup during the electron emission process that is induced by exposition to the X-ray source [3,4]. This phenomenon, called differential charging, causes energy shifts or distortion of the electron lines recorded for the elements [5]. The latter impedes a correct interpretation of the recorded data. In particular, artificial binding energy (BE) shifts can mask true chemical shifts, i.e. those due to a difference in the chemical environment around the studied elements. As charging effects are inevitable, the use of a low energy electron beam (flood gun) permanently bombarding the sample surface is often used for charge compensation and stabilization [3–6].

The perception that differential charging is a mere nuisance starts to fade as more and more research groups investigate to understand and take advantage of this physicochemical event in materials and interface sciences [3,5–12]. For instance, in a very recent publication by Larichev et al. [13] the longstanding view that the high catalytic activity of Ru/MgO catalysts in ammonia synthesis was due to a transfer of electron density from the basic sites of the MgO support to the ruthenium nanoparticles was challenged. Indeed, the authors determined that the binding energy shifts of the Ru 3d core level, supposedly occurring as a result of such electronic interactions with different oxides (SiO_2, Al_2O_3 and MgO), were rather due to a differential charging effect occurring during the XPS analyses [13]. Gaigneaux et al. [14] discerned chemically coherent oxidation states of molybdenum in MoO_3 - α-Sb_2O_4 mixed oxide catalysts from apparent oxidation states thanks to the detection and correct understanding and interpretation of differential

* Corresponding authors at: Centro de Investigaciones en Catálisis, Parque Tecnológico Guatiguará (PTG), Km. 2 vía El Refugio, Universidad Industrial de Santander, Piedecuesta (Santander) 681011, Colombia (V. G. Baldovino-Medrano).

E-mail addresses: vicbaldo@uis.edu.co (V.G. Baldovino-Medrano), eric.gaigneaux@uclouvain.be (E.M. Gaigneaux).

https://doi.org/10.1016/j.apsusc.2018.12.269
Received 30 November 2018; Accepted 28 December 2018
Available online 29 December 2018
0169-4332/

charging effects. Genet et al. [8] profited from differential charging to characterize *Azolla* leaves by XPS. Other cases illustrating the beneficial use of differential charging in materials characterization, formerly recognized by the group of Barr [7], have been highlighted in a edition of the Journal of Electron Spectroscopy and Related Phenomena. [6]

In an attempt to understand the molecular-level influence of graphite as a shaping agent for heterogeneous catalysts [15,16], our group has performed a detailed XPS characterization of graphite tableted bismuth molybdate (BiMo-G) and vanadium – aluminum mixed (hydroxides) (VAlO-G) catalysts. The analysis of the set of XPS data recorded on BiMo-G and VAlO-G indicated systematic BE shifts as well as changes in the shape of the C 1s peak with the increase in graphite loading [17,18]. Both observations are recognized symptoms of differential charging expected to occur in heterogeneous materials made of conductive metallic phases supported on an insulator oxide. [7] These findings drew our attention to the possible electronic interactions that graphite can establish with different types of oxide "*substrates*". Despite the humongous amount of published literature on carbon nanotechnology, differential charging effects during the XPS analysis of graphite based materials have been seldom mentioned [19,20]. Furthermore, to the best of our knowledge, a systematic XPS study on the possible presence of differential charging effects in graphite has not been presented so far. Therefore, we decided to perform a series of XPS analyses on samples of the commercial pyrolytic graphite previously employed in our investigations. [17,18] These studies revealed some new interesting features on the presence of trace insulator impurities and their electronic interaction with pyrolytic graphite.

2. Experimental methods

Extra pure pyrolytic graphite (G) in the form of fine powder (particle size < 50 μm) was purchased from Merck (product number 104206) and used as received. According to the manufacturer, this product is obtained after heating a mixture of high quality coke, pitch, and special tars at 3273 K under the exclusion of oxygen [21]. The pyrolytic graphite thus obtained is further broken and ground in ball mills for particle size reduction. For our study, some grams of this graphite powder were calcined in a static oven at 773 K during 4 h under air. Samples of non-calcined graphite were designated as G-NC whereas those of calcined graphite were designated as G-C.

XPS measurements were carried out on a SSX 100/206 photoelectron spectrometer from Surface Science Instruments (USA) equipped with a monochromatized micro focused Al X-ray source (powered at 20 mA and 10 kV), a 30° solid angle acceptance lens, a hemispherical analyser and a position sensitive detector. Powder samples were pressed into small stainless steel troughs of 4 mm diameter and then mounted on a multi-specimen sample-holder. Two types of sample holders were employed: a metallic aluminium carousel and a home-made ceramic carousel (Macor® Switzerland). In both cases, a grounded nickel grid was fixed to the support of the sample holder and placed 3 mm above the sample surface for charge stabilization. Samples were introduced in the preparation chamber and kept overnight at a pressure of ca. 10^{-5} Pa before transferring them to the analysis chamber of the apparatus. The pressure in the analysis chamber was around 10^{-6} Pa. The angle between the surface normal and the axis of the analyzer lens was 55°. The analyzed area was approximately 1.4 mm^2 (an ellipsoid spot of 1000 μm × 1700 μm) and the pass energy was set at 150 eV for survey scans and 50 eV for narrow scans. In the latter conditions, the full width at half maximum (FWHM) of the Au $4f_{7/2}$ core level of a clean gold standard sample was ca 1.1 eV. Data treatment was performed with the CasaXPS program (Casa Software Ltd, UK), and the acquired spectra were decomposed with a Gaussian/Lorentzian (85/15) product function after subtraction of a Shirley baseline. Molar fractions were calculated using peak areas normalized on the basis of acquisition parameters and sensitivity factors provided by the manufacturer [mean free path varying according to the 0.7th power of the photoelectron kinetic energy;[22] Scofield cross sections;[23] transmission function assumed to be constant]. Given that the spectra were recorded under different experimental conditions, the following nomenclature was adopted: Element peak (No. of scans; acquisition time [min]; pass energy [eV]; flood gun energy [eV]). e.g., Survey scan (30; 110.1; 150; 6) means that a survey scan was registered using 30 scans during 110.1 min at a pass energy of 150 eV and operating the flood gun at 6 eV.

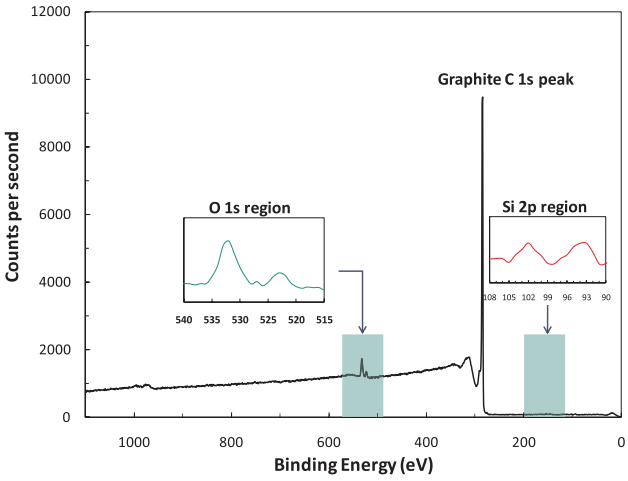

Fig. 1. Survey scan (30; 110.1; 150; 6) recorded for a sample of non-calcined graphite on a metallic sample holder.

3. Results

Results concerning the exploitation of differential charging effects for quantification and chemical identification of impurities in graphite are presented below.

3.1. General features and elemental quantification of the studied samples

A first series of spectra for samples of non-calcined and calcined graphite mounted on the metallic carousel were recorded. Fig. 1 shows a Survey scan (30; 110.1; 150; 6) for a sample of non-calcined graphite. Besides the C 1s peak of graphite, the presence of oxygen and silicon was determined on both non-calcined and calcined graphite (see inserts). It is worth mentioning that the signal of the silicon peak was not distinguished from experimental noise for an acquisition time lower than 110.1 min. Both oxygen and silicon displayed two well separated peaks. In Fig. 1, the first oxygen peak was centered at about 532.0 eV and the second one at about 523.0 eV. For silicon, the first peak was centered at ca. 102.0 eV and the second at ca. 93.0 eV. The oxygen and silicon peaks registered at higher binding energy values were thereafter named O 1s – A and Si 2p – A, and the peaks registered at lower binding energy O 1s – B and Si 2p – B. On the basis of the above results, the following sequence of spectra was recorded for four samples issued from non-calcined graphite and three samples issued from calcined graphite: C 1s (3; 14.5; 50; 6); O 1s (16; 26.4; 50; 6); and, Si 2p (128; 171.6; 50; 6). Measurements were performed in different days. During the Si 2p (128; 171.6; 50; 6) measurements, additional Al 2 s and Al 2p peaks were detected. These peaks were labeled following the same nomenclature as the one for the peaks of oxygen and silicon. Fig. 2(a) and (b) show the acquired O 1s and Si 2p spectra; the latter containing the aluminium peaks. The average elemental quantification of the samples is presented in Table 1. The total molar carbon content associated to graphite was rather constant, ca. 96.8 mol%, for G-NC and G-C. Accordingly, the total concentration of oxygen plus silicon plus aluminium remained below 4.0 mol%. The fact that calcination (T = 773 K, ambient air) did not substantially modify the molar

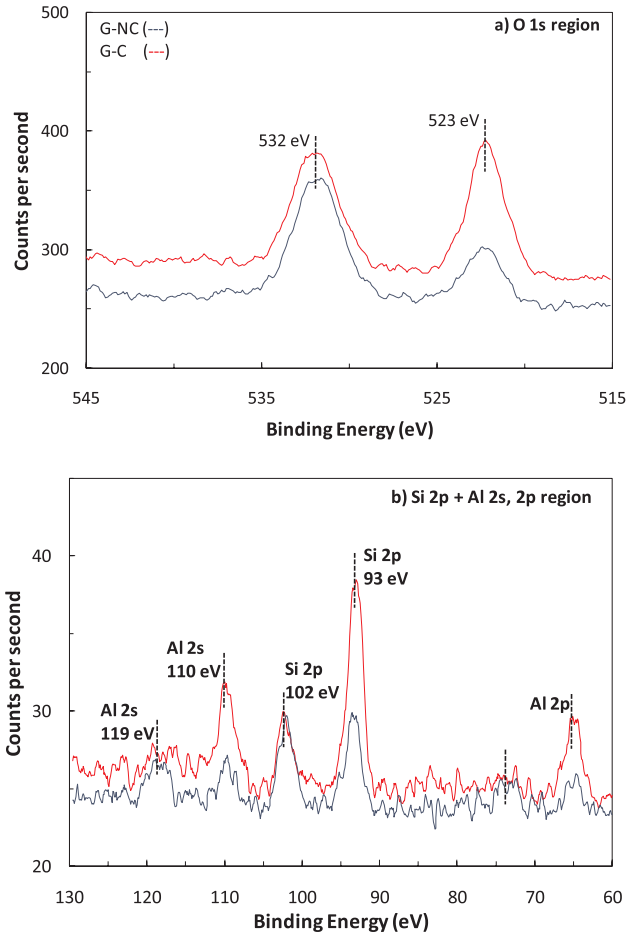

Fig. 2. High resolution spectra of oxygen and silicon: (a) O 1s (16; 26.4; 50; 6); and (b) Si 2p (128; 171.6; 50; 6) for selected samples of non-calcined (G-NC) and calcined (G-C) graphite mounted on a metallic sample holder. Spectra smoothed for presentation.

Table 1
Quantitative XPS analysis for four samples of non-calcined graphite and three samples of calcined graphite. *No peak decomposition was performed during quantification. **The FWHM value of components Al 2p – A and – B were set at the same value during peak decomposition. †Quantified from a C 1s (150; 350.3; 50; 3) peak recorded in extended experiment. STD = Mole% standard deviation. ND = not determined.

Sample	Peak	BE (eV)	ΔBE (eV)	FWHM (eV)	Mole %	STD
G-NC	Graphite	284.4	9.8	1.2	96.78	0.46
	Adv. carbon*,†	274.6		3.2	0.34	ND
	O 1s – A	532.1	9.0	3.4	1.96	0.48
	O 1s – B	523.1		2.7	0.56	0.08
	Si 2p – A	102.3	8.3	2.6	0.19	0.03
	Si 2p – B	94.1		2.7	0.20	0.02
	Al 2 s,p** – A	74.3	9.1	2.5	0.12	0.07
	Al 2 s,p** – B	65.2		2.5	0.09	0.02
G-C	Graphite	284.4	N.D.	1.1	96.76	0.43
	O 1s – A	532.0	8.8	3.3	1.16	0.23
	O 1s – B	523.2		2.5	1.24	0.18
	Si 2p – A	102.2	8.0	3.0	0.16	0.02
	Si 2p – B	94.2		2.3	0.39	0.06
	Al 2s*	111.0	N.D.	1.9	0.30	0.04

composition of graphite indicates that such treatment does not lead to a decomposition of its graphene layers. This is in agreement with our previous studies on the use of graphite as a shaping agent of catalytic powders. [17,18] The only remarkable effect of calcination on the molar composition of G-NC and G-C was a shift in the relative concentrations of oxygen, silicon, and aluminium. Thus, the ratio (O 1s – A)/(O 1s – B) decreased from 3.5 to 0.9 after calcination, while the ratio (Si 2p – A)/(Si 2p – B) decreased from 1.0 in G-NC to 0.4 in G-C. A chemical interconversion of the oxygen, silicon, and aluminium species from those registered at higher binding energy to those at lower binding energy is thus suggested because the total molar concentration of the elements remained rather constant. It is interesting to observe that the distance (ΔBE) between the O 1s – A, O 1s – B, Si 2p – A, Si 2p – B, and Al 2p, s – A, Al 2p, s – B peaks was very similar in all cases (8.0 – 9.0 eV). Furthermore, the oxygen, silicon, and aluminium peaks registered at lower binding energies did neither match the compounds reported in relevant literature, [8,17,31–33,18,24–30] nor those reported in recognized XPS databases [34–36]. As it will be demonstrated in the subsequent section, such peaks appear due to differential charging effects.

3.2. Differential charging effects on graphite samples

The results of the experiments presented herein demonstrate that differential charging effects are responsible for the presence of the oxygen, silicon, and aluminium peaks registered at 523.1; 94.1; and 65.2 eV, respectively.

If the above statement is true, the presence of a charged peak of adventitious carbon associated to the charged silicon and aluminium species can be expected to appear at a ΔBE value similar to that registered between the peaks A and B of oxygen, silicon, and aluminium. A special long duration experiment was thus devised to detect such adventitious C 1s peak. A sample of G-NC was chosen as representative for the ensemble of graphite samples. The following sequence of spectra was recorded: Survey scan (4; 14.8; 150; 6), C 1s (150; 350.3; 50; 6), O 1s (30; 30.6; 50; 6), and Si 2p (150; 350.3; 50; 6). The insert featured in Fig. 3 displays the C 1s peak of adventitious carbon registered during this experiment. The molar concentration of this carbon species was 0.34 mol%, with a FWHM of 3.2 eV and a ΔBE; in regard to the C 1s peak of graphite, of 9.8 eV (Table 1). This value was close to the ΔBEs for the oxygen, silicon and aluminium peaks previously determined. Consequently, this peak can be indeed attributed to adventitious carbon species subjected to differential charging under the present experimental conditions. It is noticeable that the concentration of adventitious carbon (0.34 mol%) is up to ca. 60% of the concentration of silicon plus aluminium. Normally, the level of adventitious carbon measured in XPS for silicon and aluminium oxides, as well as for other inorganic oxides, is in the 10 to 20% range. [17,18,24,37,38] Therefore, part of the charged adventitious carbon is associated to graphite

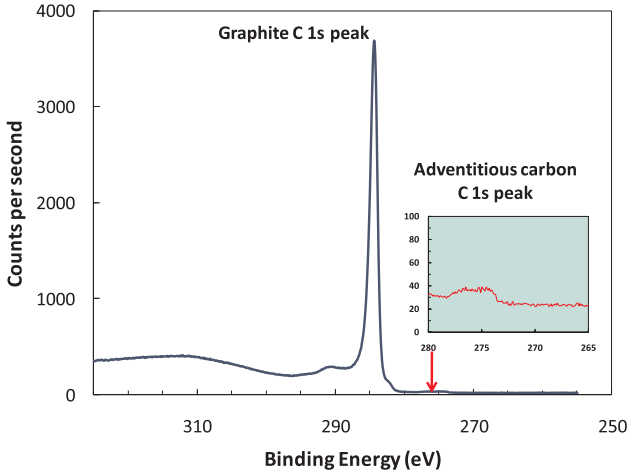

Fig. 3. High resolution C 1s (150; 350.3; 50, 6) spectrum registered in a long duration experiment for a selected sample of non calcined graphite.

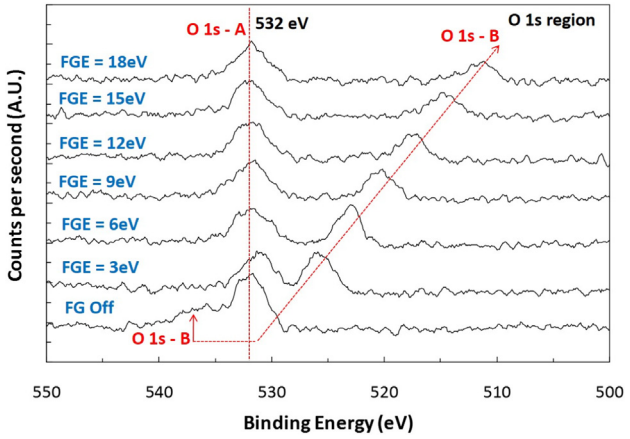

Fig. 4. O 1s peaks of a sample of calcined graphite analyzed as a function of flood gun energy (FG).

itself.

A second experiment was designed to study the differential charging of the impurities. It consisted on determining the effect of the energy of the flood gun device on the spectra of carbon and oxygen. Both types of samples, G-NC and G-C, were examined. The flood gun energy (FG) was varied between from FG = Off to FG = 18 eV and vice versa so as to complete a cycle. Fig. 4 presents the evolution of the position, as referred to the binding energy scale, of the O 1s peaks as a function of FG. The featured data correspond to a sample of G-C for which the C 1s (1; 2.2; 50; FG = Off – 18) and the O 1s (8; 18.5; 50; FG = Off – 18) peaks were recorded. In the figure, a single peak is observed when FG = Off. This peak can be decomposed into a main component centered at ca. 532 eV (O 1s – A) and a wider one extending to a higher binding energy (O 1s – B). The component O 1s – B split from the component O 1s – A; which always kept its original BE center, with the increase in FG then becoming a completely separate peak. Such split was reversible and the peak O 1s – B returned to its original binding energy position at the end of the cycle. Fig. 5 is a plot of the charging term (Ec) for the peak O 1s – B versus FG, and it demonstrates the linear variation of the former during the cycle and the reversibility of the effect of the variation of FG on the position of the O 1s – B peak. A comparison of the values of the relative percentage areas of the peaks O 1s – A and O 1s – B shows that in the range of FG values 6–12 eV the variability in the quantification is less important (Table 2). It is worthwhile noticing that the FWHMs of the peaks O 1s – A and O 1s – B reach values that do not surpass 4.1 eV under these conditions. Particularly, the FWHM of the charged oxygen

Table 2
Relative peak areas and FWHM values for the O 1s line of a sample of calcined graphite as a function of FG (eV). O 1s – A = oxygen component at 532 eV; O 1s – B = oxygen peak displaced as a function of FG.

FG (eV)	Relative peak area (%)		FWHM (eV)	
	O 1s – A	O 1s – B	O 1s – A	O 1s – B
Off	61.2	38.8	2.9	5.0
3	53.9	46.1	3.3	2.7
6	59.3	40.7	4.0	2.4
9	63.5	36.5	4.1	3.0
12	65.8	34.2	3.6	2.7
15	63.4	36.6	3.3	3.1
18	71.2	28.8	3.6	2.8
18	66.8	33.2	3.5	2.9
15	69.7	30.3	3.1	2.1
12	57.7	42.3	3.4	3.1
9	56.9	43.1	3.4	2.4
6	54.9	45.1	3.2	2.6
3	49.0	51.0	3.3	2.3
Off	41.9	58.1	4.1	3.1

peak diminished from 5.0 eV, FG = Off at the beginning of the cycle, to a maximum of 3.1 eV within the aforementioned FG range. Furthermore, one may observe that the FWHM of the peaks is lower in the second part of the cycle, i.e. when FG is diminished from 18 eV to Off. This suggests that charge distribution is more homogeneous over the samples during the second part of the cycle. A factor that can be playing a role on this fact is the accumulation time and its effect on a possible degradation of the samples during the experiment. To study this variable, the evolution of the concentration of oxygen and carbon as a function of the accumulation time was performed by fixing FG = 6 eV. The peaks O 1s (16; 26.4; 50; 6) and C 1s (3: 5.1; 50; 6) were sequentially registered during ca. 500 min for both G-NC and G-C. Fig. 6 displays the obtained results in terms of the calculated oxygen to carbon and O 1s – A to O 1s – B ratios. Though some fluctuation in the values of the aforementioned ratios was registered, one can say that, in general, both ratios remained rather constant provided the numerical error inherent to data treatment. This is more noticeable in the case of the (O 1s – A)/(O 1s – B) ratio for which the signal to noise ratio is larger. The registered trend thus indicates that graphite samples do not degrade under the present experimental conditions. Conversely, and recalling Table 2, it is suggested that the conditions at which the flood gun device is operated can impact the elemental quantification of the sample despite its no degradation.

All of the above evidence clearly demonstrates the existence of two chemical species associated to oxygen, silicon, and aluminium. Such

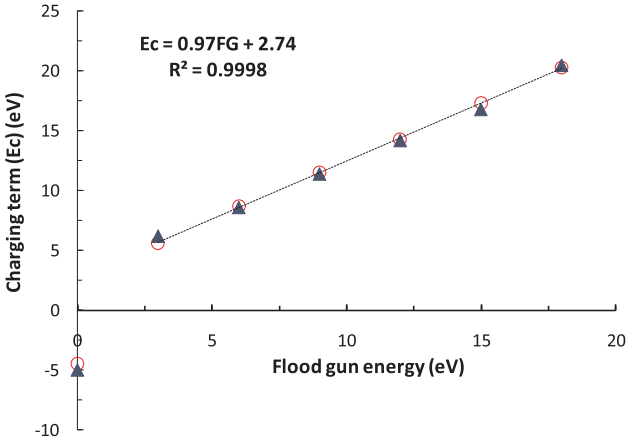

Fig. 5. Charging term ($E_c = h\upsilon - E_k - E_b$) for the O 1s - B peak of calcined graphite plotted as a function of the applied FG. ○ = during FG increase; ▲ = during FG decrease. The value 0 eV was assigned to FG = Off.

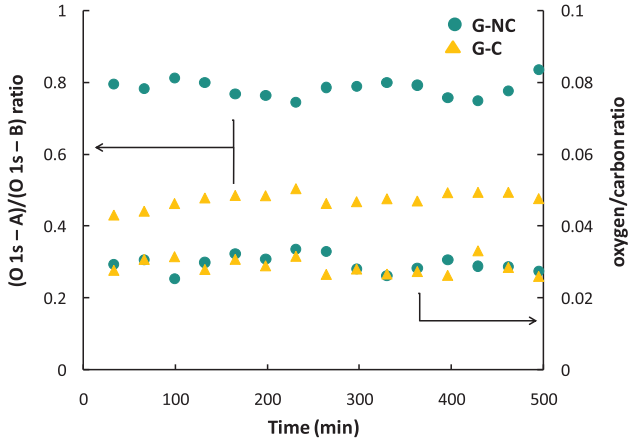

Fig. 6. Evolution of the oxygen/carbon and (O 1s – A)/(O 1s – B) mole ratios as a function of accumulation time. O 1s – A = oxygen peak at ca. 532 eV; O 1s – B at ca. 523 eV. Samples were analyzed on a metallic sample holder at FG = 6 eV.

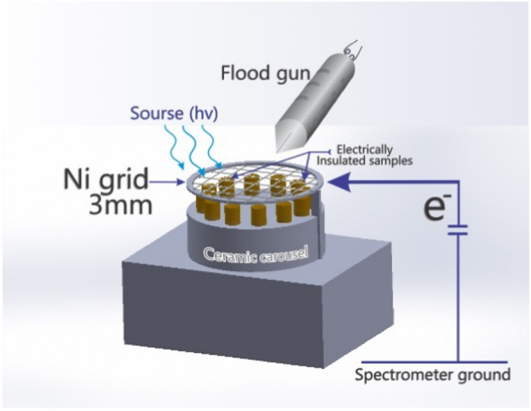

Fig. 7. Schematic representation of XPS sample analysis using a ceramic carrousel isolated from the spectrometer.

species possess different electrical conductivities that lead to a differential charging effect during XPS examination. The following section is devoted to establishing the chemical identity of such species.

3.3. Identification of chemical species

A strategy to circumvent differential charging effects during the analysis of insulator materials is to electrically isolate the samples from the spectrometer. The stabilization of the surface charge of the sample is thus achieved by combining the flood gun device plus the placement of a conductive metallic grid at a given height above the samples. The latter is in turn electrically grounded to the spectrometer [39]. Following such strategy, the analysis of the noncalcined and calcined graphite samples was performed using the experimental set-up commonly employed for the examination of insulator samples in our laboratory [17,18,24,37,38]. Fig. 7 schematizes the way in which samples are set inside the analysis chamber of the spectrometer under the above conditions. The set-up is similar to the one employed with the metallic carousel but for the fact that FG = 8 eV. The utilization of the ceramic sample holder induces a stable differential charging effect which allows a distinction of the chemical species present in the sample [8]. Conversely, a reference peak position is required to correct the binding energy scale. Considering the results of the analyses performed over the metallic sample holder, the C 1s peak of graphite at 284.4 eV was chosen as reference [40,41]. The peaks C 1s (16; 26.4; 50; 8) and O 1s (16; 16.3; 50; 8) were recorded in this case. Fig. 8 displays representative O 1s peaks recorded for both noncalcined and calcined

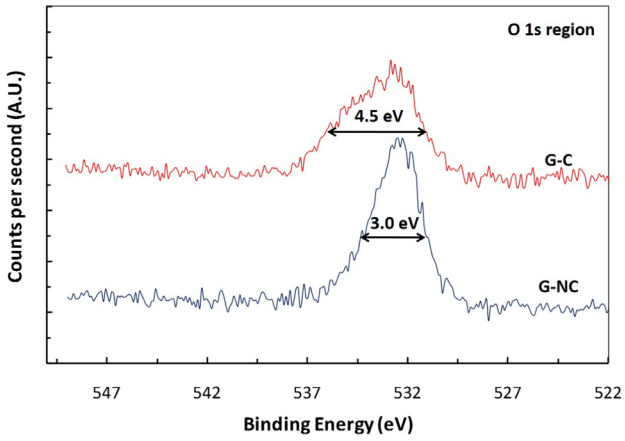

Fig. 8. High resolution O 1s (16; 16.3; 50; 8) peaks for noncalcined and calcined graphite samples as recorded on a ceramic carousel at FG = 8 eV. The BE scale was corrected in regards to the graphite C 1s peak at 284.4 eV.

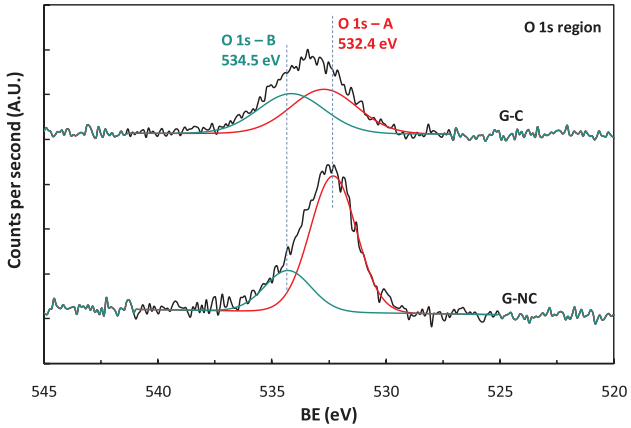

Fig. 9. Decomposition of the O 1s peak of noncalcined and calcined graphite recorded on a ceramic carousel (FG = 8 eV). The BE scale was corrected in regards to the graphite C 1s peak at 284.4 eV.

graphite samples. As expected, no peak splitting was observed. A change in both the symmetry and FWHM of the O 1s peak is clearly seen when comparing calcined graphite (FWHM = 3.0 eV) to noncalcined graphite (FWHM = 4.5 eV). Both peaks showed their summit at ca. 532 eV which agrees with the position of the O 1s – A peak registered over the metallic sample holder. Considering the results of the quantification performed for the O 1s – A and O 1s – B registered over the metallic sample holder (Tables 1 and 2), a decomposition of the O 1s peak registered over the ceramic carousel, i.e. free of differential charging effects, is proposed by imposing the following restrictions: (i) O 1s – B (FWHM) = O 1s – A (FWHM), (ii) Area of O 1s – B = 0.3*(Area of O 1s – A) for G-NC, and (iii) Area of O 1s – B = 0.9*(Area of O 1s – A). The (O 1s – B)/(O 1s – A) ratios were derived from the values reported in Table 2. Fig. 9 shows the decomposition of the O 1s peak chosen as representative of three samples of noncalcined and three samples of calcined graphite. According to the proposed decomposition, the peak O 1s – A was centered at ca. 532.4 ± 0.1 eV and the peak O 1s – B at ca. 534.4 ± 0.3 eV for both noncalcined and calcined graphite. The FWHM values of the components increased from 2.6 ± 0.2 eV for noncalcined graphite to 3.2 ± 0.3 eV for calcined graphite. According to Hontoria-Lucas et al.,[42] the component at 532.4 ± 0.1 eV, i.e. O 1s – A, is associated to the sum of the contributions of oxygen doubly bound to carbon, particular, oxygen chemically bonded to aromatic groups and aliphatic structures. A consultation of the databases [35,36] further confirms that such oxygen species should be mostly associated to oxygen – carbon bonds in organic type compounds or to oxygen associated to inorganic hydroxyls (–OH). According to literature [43], the peak O 1s – B is found to be located at a binding energy reported for oxygen making part of inorganic insulator metallic oxides such as SiO_2 and Al_2O_3. Consequently, the peaks O 1s – A and O 1s – B will be henceforward identified as O–[C,OH] and O–MO_x (MO_x = metal oxide), respectively. On the other hand, a correlation of the differential charging effect registered for oxygen, silicon, and aluminium sheds light on the chemical identity of the peaks Si 2p – A, Si 2p – B, Al 2p – A, and Al 2p – B. On one hand, the peak Si 2p – A at 102.3 eV has been ascribed to silicon in silicone polymeric structures [44–46] and to silicon in alumino-silicate oxides (Al_2OSiO_4) such as clays [35,36]. From our results, it is not possible to affirm which one of the above is the precise compound present on the samples. But the aluminium to silicon ratio of the samples (Si 2p – A/Al 2p – A (G-NC) = 1.6) suggests that both silicone and Al_2OSiO_4 could be present. Silicone has been reported as a possible ambient contaminant in laboratory samples [26]. It can come from sample handling and storage in conventional desiccators. Taking into account the information provided by the manufacturer [21], the most probable source of contamination for the analyzed graphite is the ball milling process where its particle size is reduced.

Conventional grinders use ceramic balls containing clays susceptible to be transferred to the processed materials in very small concentrations. Moreover, it has been demonstrated that aerobic milling of graphite can lead to its partial oxidation [47]. Despite the scope of this work does not encompass a decomposition of the C 1s peak, the presence of oxygen functional groups on graphite can be clearly identified from the shoulder of the peak between 286 and 290 eV (Fig. 3). At the same time, the milling process can promote the intercalation of extraneous compounds within the graphene layers of graphite [47]. The correlation between the peaks O 1s – B, Si 2p – B, and Al 2p – B suggests the presence of insulator metallic oxides such as SiO_2 and Al_2O_3. From the elemental quantification for G-NC presented in Table 1, the theoretical molar concentration of oxygen contained in SiO_2 and Al_2O_3 can be calculated as: 2 × 0.20 (Si 2p – B mole%) + (3/2) × 0.09 (Al 2p mole %) = 0.54 mol%. This value is very close to the concentration of O 1s – B (0.56 mol%), thus supporting our hypothesis that the peaks O 1s – B, Si 2p – B, and Al 2p – B, which experienced the differential charging effect, correspond to SiO_2 and Al_2O_3.

4. Discussion

Differential charging effects are inherent to the XPS examination of insulators. According to Bryson [39], they result from a net positive charge generated on the sample surface during the photoemission process and from a simultaneous potential gradient across the sample surface. A way to circumvent the problems derived from differential charging is to irradiate the studied samples with a low energy electron source; namely, the so-called flood gun device [39,48]. Such devices are nowadays omnipresent in spectrometers equipped with microfocused X-ray sources. The evidence presented herein demonstrated the existence of differential charging effects in commercial graphite when a metallic sample holder is employed. The registered differential charging effect was exploited to identify two different chemical species associated to oxygen, silicon, and aluminium by means of a systematic assessment of the energy of the flood gun on the binding energy of the analyzed elements. The chemical identity of the compounds was established from the fact that the O 1s, Si 2p, and Al 2p core levels split into two peaks as a function of FG. More precisely, one of the two peaks registered for the aforementioned elements did not shift from its original position during the experiment; as it was the case for the graphite C 1s peak. Meanwhile, the position of the second oxygen, silicon, and aluminium peaks shifted proportionally to FG.

A large difference in the electrical conductivity of the constituents of heterogeneous materials will induce a marked differential charging effect during XPS analysis. Especially, if the specimens are directly grounded to the spectrometer; which is the case when one uses a metallic sample holder. Under these conditions, such differential charging cannot be fully controlled because it often follows a rather random behavior [49]. When a ceramic sample holder is employed, the samples are no longer grounded to the spectrometer. The use of the flood gun is thus mandatory for signal acquisition and a net controlled charging effect is induced on the ensemble of the specimens. Because of this, chemical speciation becomes reliable, since it solely depends on true chemical shifts due to changes in the chemical environment of the elements. Therefore, one can easily distinguish chemical species after selecting an appropriate reference peak for correcting the binding energy scale [28]. From a comparison of the data recorded over the two types of sample holders, it was herein possible to conclude that the shifted peaks corresponded to SiO_2 and Al_2O_3. The trends registered over the metallic sample holder are due to the fact that SiO_2 and Al_2O_3 are insulators whereas graphite is a semiconductor. Nevertheless, this explanation falls short when considering the peaks of oxygen, silicon, and aluminium that did not shift during the FG variation experiments. Recalling the results obtained over the ceramic sample holder, these peaks can be attributed either to silicone or to an alumino-silicate oxide. As previously stated, our results do not allow affirming if one or both compounds are present in the samples. What is true is that both types of compounds are electrical insulators as it is the case of SiO_2 and Al_2O_3. In the case of silicone and SiO_2, the difference in their behavior cannot be explained from arguments related to the ionic character of the corresponding Si—O bonds because their values are very close to each other: the Si—O backbone bonds in silicone have a 51% ionic character [50] while the Si—O bonds have an ionic character of ca. 45% [51]. Therefore, such argument must be ruled out. An alternative explanation involves a geometrical effect as considered from an electrostatic point of view. The theoretical mechanisms for differential charging postulated by Cazaux [5] point out the important role of geometry in describing the electrostatic phenomena involved during the photoelectron emission process. The specific role of the spatial heterogeneities of the sample on the developed surface potential is addressed therein [5]. Considering the history of the graphite samples studied herein, one can suppose that the differential charging effect is related to a geometric effect. Indeed, the impurities within the samples that did not experience charging effect were ascribed to silicone and/or ceramic clay coming from the grinding step of graphite. Silicone is a generic name for a family of linear cross-linked polymers [52] that can easily intercalate within the laminar graphite structure. Similarly, ceramic clays are laminar arrangements of alternating SiO_4 – AlO_4 structures [53] that share a geometric resemblance with graphite. It can be imagined that the electrical behavior of a mixture graphite - silicone/ceramic clay is analogous to the electrical behavior of a parallel-plate capacitor (Fig. 10a). In such a configuration, a rather homogeneous and electrical charge of the material would ensure the continuous conduction of electrons from the spectrometer ground to the sample; like in a conventional direct current electrical circuit. Conversely, SiO_2 and Al_2O_3 form spherical and plate like shape particles [17], respectively, that would produce a quite different electrical configuration during XPS examination (Fig. 10b). SiO_2 and Al_2O_3 particles would present electrical interactions between each other that would lead to interparticle surface charging effects.

Finally, a tentative explanation for the increase in the concentration of SiO_2 and Al_2O_3 for calcined graphite (Table 1) can be provided when considering that a transformation of silicone into SiO_2 could have occurred during calcination. It has been established that, under oxidation conditions at 773 K, silicone decomposes into SiO_2, CO_2, and water [54]. It is also possible that a dehydroxylation and sintering of the ceramic clay contaminant during calcination [55] would contribute to such increase because of an additional differential charging effect. Nevertheless, such explanations are far from being complete and future experimentation in this direction in required.

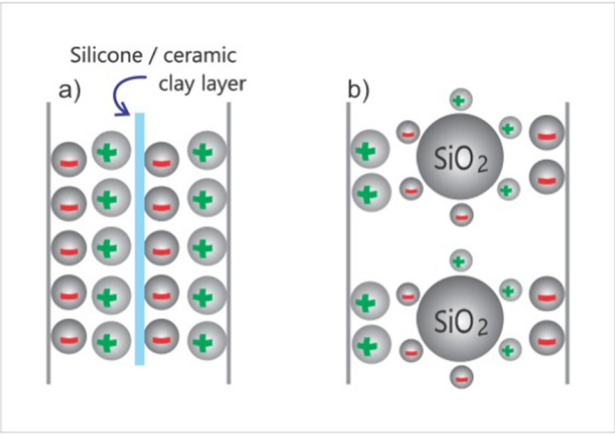

Fig. 10. Schematic representation of the surface charge distribution between: (a) silicone/ceramic clay and graphite, (b) silica particles and graphite.

5. Conclusions

XPS differential charging effects were exploited for the assessment of the chemical nature and concentration of impurities (oxygen, silicon, and aluminium) in commercial pyrolytic graphite. Samples of non-calcined (as received) and calcined graphite were systematically analyzed under different conditions in XPS. The study of the effect of the energy of the flood gun device on the positions of the peaks O 1s, Si 2p, and Al 2p over specimens mounted on a metallic sample holder led to a clear distinction of two different chemical species associated to the above elements. Further analysis of the samples over a ceramic sample holder (i.e. samples electrically isolated from the spectrometer ground) allowed identifying SiO_2, Al_2O_3, silicone/alumino-silicate oxide clays as insulator inorganic contaminants of the semiconductive graphite samples. Data treatment of the peaks recorded on the metallic sample holder served as a basis to establish some constraints for the decomposition of the peaks associated to the above compounds. The FWHM values and the relative concentration of the chemical species ascribed to the peaks presenting the differential charging were of particular interest. To explain differential charging of the impurities, a model based on electrical analogies and geometrical considerations was postulated. This model considered charge distribution over particles of silicone/alumino-silicate oxide clays and SiO_2 and Al_2O_3 which have different shapes.

Acknowledgements

This work was done within the frame of the IAP P6/17 “Inanomat” project entitled “Advanced complex inorganic materials by a novel bottom-up nanochemistry approach: processing and shaping” funded by Belspo (Belgium). Authors thank FNRS for funding XPS experiments and Professor Paul Rouxhet for fruitful discussions. Authors especially thank Michel J. Genet for his valuable insights into the paper. Víctor G. Baldovino-Medrano thanks the Fonds Speciaux de Recherche (UCL) and the Marie Curie Actions of the European Commission for his post-doctorate fellowship. R. Ospina thanks Vicerrectoría de Investigaciones y Extensión – UIS for funding within the frame of its program for post-doctoral stays.

References

[1] B. Siegbahn, K. Siegbahn, K. Nordling, C. Fahlman, A. Nordberg, R. Hedman, J. Johannson, G. Bergmark, T. Karlsson, S. Lindgren, T. Lindberg, ESCA: Atomic, Molecular and Solid State Structure Studied by Means of Electron Spectroscopy, Almqvist and Wiksell, Uppsala, 1967.

[2] A.J. Roberts, C.E. Moffitt, Trends in XPS instrumentation for industrial surface analysis and materials characterisation, J. Electron Spectros. Relat. Phenomena. (2018), https://doi.org/10.1016/j.elspec.2018.03.002.

[3] R.C.M. Liehr, P.A. Thiry, J.J. Pireaux, Characterization of insulators by high-resolution electron-energy-loss spectroscopy: application of a surface-potential stabilization technique, Phys. Rev. 33 (1986), https://doi.org/10.1103/PhysRevB.33.5682.

[4] K. Kayed, Effect of nitrogen plasma afterglow on the surface charge effect resulted during XPS surface analysis of amorphous carbon nitride thin films, Spectrochim. Acta Part A Mol. Biomol. Spectrosc. (2018), https://doi.org/10.1016/j.saa.2018.03.076.

[5] J. Cazaux, Mechanisms of charging in electron spectroscopy, J. Electron Spectros. Relat. Phenomena. 105 (1999) 155–185, https://doi.org/10.1016/S0368-2048(99)00068-7.

[6] P.M.A. Sherwood, Preface, J. Electron Spectros. Relat. Phenomena. 176 (2010) 2–4, https://doi.org/10.1016/j.elspec.2009.10.005.

[7] T.L. Barr, Studies in differential charging, J. Vac. Sci. Technol. A Vacuum, Surf. Film. 7 (1989) 1677–1683, https://doi.org/10.1116/1.576069.

[8] M.J. Genet, C. Jacques, N. Mozes, C. Van Hove, A. Lejeune, P.G. Rouxhet, Use of differential charging to analyse microscopic specimens of Azolla leaves by XPS, Surf. Interf. Anal. 33 (2002) 601–606, https://doi.org/10.1002/sia.1427.

[9] S. Mukherjee, M. Mukherjee, Controlled surface neutralization: a quantitative approach to study surface charging in photoemission, J. Electron Spectros. Relat. Phenomena 154 (2007) 90–95, https://doi.org/10.1016/J.ELSPEC.2006.12.038.

[10] V.I. Bukhtiyarov, I.P. Prosvirin, R.I. Kvon, Application of differential charging for analysis of electronic properties of supported silver, J. Electron Spectros. Relat. Phenomena 77 (1996) 7–13, https://doi.org/10.1016/0368-2048(95)02378-X.

[11] I. Doron-Mor, A. Hatzor, A. Vaskevich, T. Van Der Boom-Moav, A. Shanzer, I. Rubinstein, H. Cohen, Controlled surface charging as a depth-profiling probe for mesoscopic layers, Nature 406 (2000) 382–385, https://doi.org/10.1038/35019025.

[12] K. Shabtai, I. Rubinstein, S.R. Cohen, H. Cohen, High-resolution lateral differentiation using a macroscopic probe: XPS of organic monolayers on composite Au-SiO2 surfaces, J. Am. Chem. Soc. 122 (2000) 4959–4962, https://doi.org/10.1021/ja993710h.

[13] Y.V. Larichev, B.L. Moroz, V.I. Bukhtiyarov, Electronic state of ruthenium deposited onto oxide supports: an XPS study taking into account the final state effects, Appl. Surf. Sci. 258 (2011) 1541–1550, https://doi.org/10.1016/j.apsusc.2011.09.127.

[14] E.M. Gaigneaux, M.J. Genet, P. Ruiz, B. Delmon, Catalytic behavior of molybdenum suboxides in the selective oxidation of isobutene to methacrolein, J. Phys. Chem. B. 104 (2000) 5724–5737, https://doi.org/10.1021/jp9913416.

[15] Y. Huo, F. Yao, Y. Ma, Catalytic performance of graphite oxide supported au nanoparticles in aerobic oxidation of benzyl alcohol: support effect, Chinese J. Chem. Phys. 30 (2017) 90–96, https://doi.org/10.1063/1674-0068/30/cjcp1604088.

[16] A.F. Orrego-Romero, O.F. Arbeláez-Pérez, F. Bustamante-Londoño, A.L. Villa-Holguín, Pelletization of catalysts supported on activated carbon. A Case study: clean synthesis of dimethyl carbonate from methanol and CO2, Rev. Fac. Ing. Univ. Antioquia. (2015) 38–47, https://doi.org/10.17533/udea.redin.n78a05.

[17] V.G. Baldovino-Medrano, M.T. Le, I. Van Driessche, E. Bruneel, E.M. Gaigneaux, Influence of graphite as a shaping agent of Bi molybdate powders on their mechanical, physicochemical, and catalytic properties, Ind. Eng. Chem. Res. 50 (2011) 5467–5477, https://doi.org/10.1021/ie102473h.

[18] V.G. Baldovino-Medrano, B. Farin, E.M. Gaigneaux, Establishing the role of graphite as a shaping agent of vanadium-aluminum mixed (Hydr)oxides and their physicochemical properties and catalytic functionalities, ACS Catal. 2 (2012) 322–336, https://doi.org/10.1021/cs200465h.

[19] J.I. Parades, S. Villar-Rodil, A. Martínez-Alonso, J.M.D. Tascón, Graphene oxide dispersions in organic solvents, Langmuir 24 (2008) 10560–10564, https://doi.org/10.1021/la801744a.

[20] J. Filik, P.W. May, S.R.J. Pearce, R.K. Wild, K.R. Hallam, XPS and laser Raman analysis of hydrogenated amorphous carbon films, Diam. Relat. Mater. 12 (2003) 974–978, https://doi.org/10.1016/S0925-9635(02)00374-6.

[21] MERK, 104206 | Grafito, (2018). http://www.merckmillipore.com/belgium/chemicals/graphite (accessed April 11, 2018).

[22] W. Hanke, H. Ebel, M.F. Ebel, A. Jablonski, K. Hirokawa, Quantitative XPS — multiline approach, J. Electron Spectros. Relat. Phenomena 40 (1986) 241–257, https://doi.org/10.1016/0368-2048(86)80023-8.

[23] J.H. Scofield, Hartree-slater subshell photoionization cross-sections at 1254 and 1487 eV, J. Electron Spectros. Relat. Phenomena 8 (1976) 129–137 (accessed April 12, 2018).

[24] T.L. Barr, S. Seal, Nature of the use of adventitious carbon as a binding energy standard, J. Vac. Sci. Technol. A Vacuum, Surf., Film 13 (1995) 1239–1246, https://doi.org/10.1116/1.579868.

[25] R.I.R. Blyth, H. Buqa, F.P. Netzer, M.G. Ramsey, J.O. Besenhard, P. Golob, M. Winter, XPS studies of graphite electrode materials for lithium ion batteries, Appl. Surf. Sci. 167 (2000) 99–106 (accessed April 12, 2018), www.elsevier.nlrlocaterapsusc.

[26] V. Aguié-Béghin, Y. Adriaensen, N. Péron, M. Valade, P. Rouxhet, R. Douillard, Structure and chemical composition of layers adsorbed at interfaces with champagne, J. Agric. Food Chem. 57 (2009) 10399–10407, https://doi.org/10.1021/jf9016948.

[27] A. Bismarck, R. Tahhan, J. Springer, A. Schulz, T.M. Klapijtke, H. Zell', W. Michaeli', Influence of fluorination on the properties of carbon fibres, J. Fluor. Chem. 84 (1997) 127–134 (accessed April 12, 2018), https://ac.els-cdn.com/S0022113997000298/1-s2.0-S0022113997000298-main.pdf?_tid=dd4db1d3-7f02-4ace-80fc-553d58c06682&acdnat=1523560553_92a904484ae3fe9c902016ee4c628d87.

[28] M.J. Genet, C.C. Dupont-Gillain, P.G. Rouxhet, XPS analysis of biosystems and biomaterials, Med. Appl. Colloids (2008), https://doi.org/10.1007/978-0-387-76921-9.

[29] P. Gerin, P. Dengis, P. Rouxhet, Performance of XPS analysis of model biochemical compounds, J. Chim. Phys. 92 (1995) 1043–1065, https://doi.org/10.1051/jcp/1995921043.

[30] B.M. Weckhuysen, M.P. Rosynek, J.H. Lunsford, Characterization of surface carbon formed during the conversion of methane to benzene over Mo/H-ZSM-5 catalysts, Catal. Lett. 52 (1998) 31–36, https://doi.org/10.1023/A:1019094630691.

[31] K. Bachmann, X-ray Photoelectron Spectroscopic Studies of Carbon Fiber Surfaces. 11. Differences in the surface chemistry and bulk structure of different carbon fibers based on poly(acrylonitri1e) and pitch and comparison with various graphite samples, Chem. Mater. 2 (1990) 293–299, https://doi.org/10.1021/cm00009a020.

[32] S. Yumitori, Correlation of C1s chemical state intensities with the O1s intensity in the XPS analysis of anodically oxidized glass-like carbon samples, J. Mater. Sci. (2000), https://doi.org/10.1023/A:1004761103919.

[33] P. Brender, R. Gadiou, J.-C. Rietsch, P. Fioux, J. Dentzer, A. Ponche, C. Vix-Guterl, Characterization of carbon surface chemistry by combined temperature programmed desorption with in Situ X-ray photoelectron spectrometry and temperature programmed desorption with mass spectrometry analysis, Anal. Chem. 84 (2012) 2147–2153, https://doi.org/10.1021/ac102244b.

[34] G. Beamson, D. Briggs, High resolution XPS of organic polymers: the scienta ESCA300 database, J. Chem. Educ. 70 (1993) A25, https://doi.org/10.1021/ed070pA25.5.

[35] Y.C. Benoit, T.S. Benoit, R.D.Y. Narjoux, B. Quintana, G. Georges, XPS, AES, UPS and ESCA - lasurface.com, (2011). http://www.lasurface.com/accueil/index.php (accessed April 12, 2018).

[36] M. Gaithersburg, NIST X-ray Photoelectron Spectroscopy (XPS) Database Main Search Menu, (2003). https://srdata.nist.gov/xps/main_search_menu.aspx (accessed April 12, 2018).
[37] G.P. Babu, R.S. Murthy, Vapour phase isomerization and aromatization of C10 cyclic olefins on supported platinum catalysts, Res. Indust. 34 (1989) 273–276 (accessed April 12, 2018).
[38] D.P. Debecker, B. Schimmoeller, M. Stoyanova, C. Poleunis, P. Bertrand, U. Rodemerck, E.M. Gaigneaux, Flame-made MoO3/SiO2-Al2O3 metathesis catalysts with highly dispersed and highly active molybdate species, J. Catal. 277 (2011) 154–163, https://doi.org/10.1016/j.jcat.2010.11.003.
[39] C.E. Bryson, Surface potential control in XPS, Surf. Sci. 189–190 (1987) 50–58, https://doi.org/10.1016/S0039-6028(87)80414-4.
[40] E. Desimoni, B. Brunetti, X-ray photoelectron spectroscopic characterization of chemically modified electrodes used as chemical sensors and biosensors: a review, Chemosensors (2015) 70–117, https://doi.org/10.3390/chemosensors3020070.
[41] G. Greczynski, L. Hultman, C 1s peak of adventitious carbon aligns to the vacuum level: dire consequences for material's bonding assignment by photoelectron spectroscopy, ChemPhysChem 18 (2017) 1507–1512, https://doi.org/10.1002/cphc.201700126.
[42] C. Hontoria-Lucas, A.J. López-Peinado, J.de D. López-González, M.L. Rojas-Cervantes, R.M. Martín-Aranda, Study of oxygen-containing groups in a series of graphite oxides: physical and chemical characterization, Carbon N. Y. 33 (1995) 1585–1592, https://doi.org/10.1016/0008-6223(95)00120-3.
[43] G. Zhou, C. Xu, W. Cheng, Q. Zhang, W. Nie, Effects of oxygen element and oxygen-containing functional groups on surface wettability of coal dust with various metamorphic degrees based on XPS experiment, J. Anal. Methods Chem. 2015 (2015), https://doi.org/10.1155/2015/467242.
[44] S.H. Gao, L.H. Gao, K.S. Zhou, Super-hydrophobicity and oleophobicity of silicone rubber modified by CF4radio frequency plasma, Appl. Surf. Sci. 257 (2011) 4945–4950, https://doi.org/10.1016/j.apsusc.2011.01.001.
[45] D. Pleul, R. Frenzel, M. Eschner, F. Simon, X-ray photoelectron spectroscopy for detection of the different Si-O bonding states of silicon, Anal. Bioanal. Chem. 375 (2003) 1276–1281, https://doi.org/10.1007/s00216-003-1811-7.
[46] T. Mundry, P. Surmann, T. Schurreit, Surface characterization of polydimethylsiloxane treated pharmaceutical glass containers by X-ray-excited photo- and Auger electron spectroscopy, Fresenius. J. Anal. Chem. 368 (2000) 820–831, https://doi.org/10.1007/s002160000593.
[47] T.S. Ong, H. Yang, Effect of atmosphere on the mechanical milling of natural graphite, Carbon N. Y. 38 (2000) 2077–2085, https://doi.org/10.1016/S0008-6223(00)00064-6.
[48] B.J. Tielsch, J.E. Fulghum, Differential charging in XPS. Part I: demonstration of lateral charging in a bulk insulator using imaging XPS, Surf. Interface Anal. 24 (1996) 422–427, https://doi.org/10.1002/(SICI)1096-9918(199606)24:6<422::AID-SIA142>3.0.CO;2-G.
[49] B.J. Tielsch, J.E. Fulghum, Differential charging in XPS. Part III. A comparison of charging in thin polymer overlayers on conducting and non-conducting substrates, Surf. Interf. Anal. 25 (1997) 904–912, https://doi.org/10.1002/(SICI)1096-9918(199710)25:11<904:: AID-SIA316>3.3.CO;2-4.
[50] J.W. Krumpfer, T.J. McCarthy, Rediscovering silicones: "unreactive" silicones react with inorganic surfaces, Langmuir 27 (2011) 11514–11519, https://doi.org/10.1021/la202583w.
[51] G. Lucovsky, Electronic structure, amorphous morphology and thermal stability of transition metal oxide and chalcogenide alloys, J. Optoelectron. Adv. Mater. 3 (2001) 155–166 (accessed April 12, 2018), https://joam.inoe.ro/arhiva/pdf3_2/Lucovsky.pdf.
[52] P. Zheng, T.J. McCarthy, Rediscovering silicones: molecularly smooth, low surface energy, unfilled, UV/Vis-transparent, extremely cross-linked, thermally stable, hard, elastic PDMS, Langmuir 26 (2010) 18585–18590, https://doi.org/10.1021/la104065e.
[53] J. Davidovits, Geopolymers, J. Therm. Anal. 37 (1991) 1633–1656, https://doi.org/10.1007/BF01912193.
[54] G. Camino, S.M. Lomakin, M. Lazzari, Polydimethylsiloxane thermal degradation part 1. Kinetic aspects, Polymer (2001) (accessed April 12, 2018), https://ac.els-cdn.com/S0032386100006522/1-s2.0-S0032386100006522-main.pdf?_tid=efb70862-8d5c-48ff-8d6f-ef8e39e33b0b&acdnat=1523571010_11ac654e195d4a6f85c2e2750e200536.
[55] A. Elimbi, H.K. Tchakoute, D. Njopwouo, Effects of calcination temperature of kaolinite clays on the properties of geopolymer cements, Constr. Build. Mater. 25 (2011) 2805–2812, https://doi.org/10.1016/j.conbuildmat.2010.12.055.